A Universal Chern Model on Arbitrary Triangulations

Nigel ${\rm Higson}^{1,\,*}$ and ${\rm Emil~Prodan}^{2,\,\dagger}$

¹Department of Mathematics, Penn State University, University Park, PA 16802, USA. ²Department of Physics, Yeshiva University, New York, NY 10016, USA (Dated: October 27, 2025)

Given a triangulation of a closed orientable surface, we consider the lattice with sites at the vertices, edges and facets of the triangulation. Borrowing from mathematics literature, we introduce on this lattice a pair of tight-binding Hamiltonians derived from the boundary and Poincaré duality maps of finite simplicial manifolds. These Hamiltonians have been proved to have clean topological spectral gaps carrying non-trivial Chern numbers in the limit of infinite refinement of the triangulation. We confirm this via numerical simulations, and demonstrate how these models enable topological edge modes at the surfaces of real-world objects. Furthermore, we describe a metamaterial whose dynamics reproduces that of the proposed model, thus bringing the topological metamaterials closer to real-world applications.

The Haldane model [1] is the prototypical example of a topological insulator from class A of the classification table of topological insulators and superconductors [2–5]. Indeed, any other topological Hamiltonian from this class on a uniform discretization of the plane can be adiabatically deformed into decoupled layers of Haldane Hamiltonians [6]. It will be useful to have something similar on discretizations of generic smooth orientable surfaces, more specifically, on any of their triangulations. We want to clarify from the start that, when dealing with compact surfaces, as we will do here, an infinite-lattice limit can be achieved by sequential refinement of the triangulations [7]. It will be in this limit where Chern numbers and bulk-boundary correspondences make rigorous sense. However the topological effects are also expected to be present for fine-enough finite triangulations, provided the topological "bulk" spectral gaps are free of defect modes.

To convey the difficulty of such a task, we display in Fig. 1 triangulations of the surface of a real-world object, highlighting the complexities and irregularities of such discrete geometries. Triangulations of surfaces of real-world objects are routinely generated by 3D scanners and, in fact, any stereolithography (stl) file inputted to a 3D printer or to any other computer numerical controlled (CNC) machine contains a triangulation of a surface. It is therefore natural to ask whether such triangulations can be decorated with suitably coupled resonators that exhibit topological collective dynamics or, more concretely, if we can deploy defect-free topological metamaterials on the surfaces of real-world objects.

When it comes to topological materials, the materials science community is trapped in Flatland, as it lacks an algorithm to generate the equivalent of the Haldane model on such discrete geometries. In fact, it is not even clear how to generate a gapped Hamiltonian free of defect-states inside the gap. In this letter, we draw attention to the pure mathematical results [9–11] by first author and John Roe, where the solution to this problem was presented as an important component of an operator-theoretic generalization of surgery theory. The central

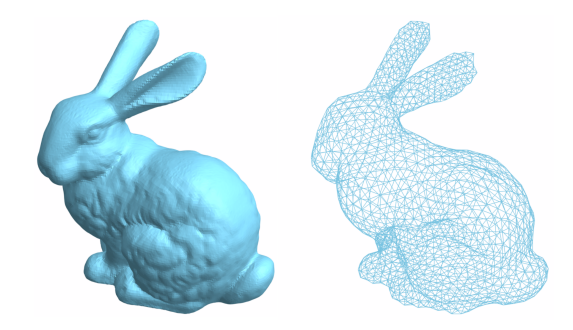


FIG. 1. Left: Stanford Bunny, a triangulated mesh containing 69,451 faces generated by a 3D scan of a ceramic figurine [8]. Right: A simplified version containing 1549 vertices, 4641 edges and 3094 faces, to be used in our computer simulations.

structures in surgery theory are CW-complexes satisfying a form of Poincaré duality or, in short, Poincaré complexes [13]. They were promoted in [9] to complexes of Hilbert spaces that admit a Poincaré duality operator, now called Hilbert-Poincaré complexes. A self-adjoint version of the duality operator and the boundary map of such complex were assembled in [9] into a pair of gapped operators over the total Hilbert space of the complex. This pair was used to define an analytic signature that is a homotopy invariant of the complex. Ref. [10] explains how to construct Hilbert-Poincaré complexes from triangulations, and this is what we will use here. Quite remarkably, in this context, the pair of gapped operators we just mentioned are local tight-binding operators that can be controlled in the infinite-lattice limit. Regardless of the surface or its triangulations, these limits always fall in the same non-trivial stable homotopy classes of projections in the Roe C^* -algebra of the plane. the algebra where the operators belong after taking the infinite-lattice limit. These classes carry precisely the Chern numbers ± 1 , a fact that can be verified computationally on a uniform triangulation of the torus.

The goals of this letter are to distill this solution down to the level of an actual meta-material and to

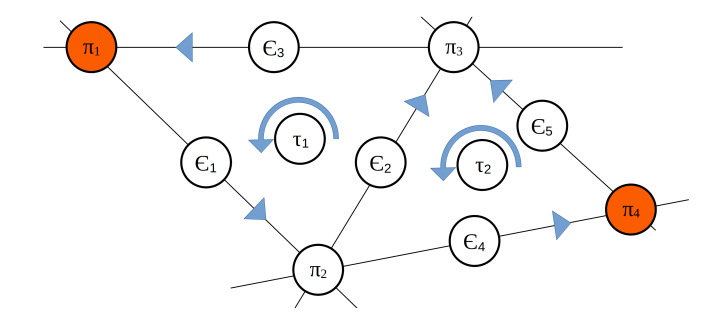


FIG. 2. A region of a triangulation and its associated data, consisting of labels and orientations of the simplices. The marked vertices and the seen orientations order the vertices of the faces as $|\tau_1\rangle = |\pi_1\pi_2\pi_3\rangle$ and $|\tau_2\rangle = |\pi_4\pi_3\pi_2\rangle$. The triangulation is populated with single-mode resonators (the disks) in a one-to-one fashion with its simplices.

demonstrate through numerical simulations the remarkable properties of the so-derived Hamiltonians. In the process, we confirm that the algorithm can be deployed on finite triangulations of real-world objects, where it produces clean topological gapped spectra. Furthermore, we confirm that, on such finite triangulations, one-way topological wave-channels can be generated on demand by simply jamming the dynamics in the regions outside of the wave-channels. The models are suited for laboratory implementations because they contain only single-mode resonators, involve only nearest-neighbor couplings, and display one and only one spectral gap of predictable size. A Mathematica® script generating the desired couplings for a given triangulation is supplied in [12].

To clarify the relation between this and other existing works, let us mention that topological gaps carrying Chern numbers can be opened by applying physical or synthetic magnetic fields perpendicular to the material's surface. While this has been demonstrated both experimentally and numerically for non-uniform discretizations of the plane, such as amorphous ones [14, 15], the (many) gaps seen in those spectra are not clean but rather small mobility gaps filled with impurity states. Furthermore, while the presence of a magnetic field can be implemented by twisting an ordinary model by the area 2-cocycle of the supporting surface[16], a process that inserts the usual Peierls factors, this will be a very difficult task for geometries as in Fig. 1. On the engineering side, such models are very difficult to work with because of the large fluctuations in the values of the couplings.

From triangulations to topological materials. A triangulation of a compact orientable surface X supplies a finite simplicial complex, made up of 2-simplices, the faces of the triangles (τ) , 1-simplices, the edges (ϵ) , and 0-simplices, the vertices (π) . Quite naturally, we associate to this data a collection of identical single-mode resonators as in Fig 2. The resonant modes carried by the p-simplices form the Hilbert space \mathcal{H}_p and the full

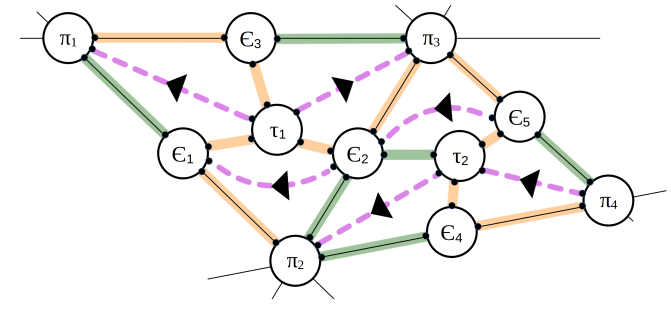


FIG. 3. Resonator couplings needed to implement the operator $B+B^{\dagger}$ (continuous thick lines), and operator S (oriented dashed lines), for the data from Fig. 2. The color coding and other conventions are explained in Fig. 4.

Hilbert space where the dynamics of the meta-material happens is $\mathcal{H} = \bigoplus_{p=0}^2 \mathcal{H}_p$. It is important that the surface is orientable, which enables us to coherently orient the 2-simplices. Additionally, the 2-simplices will be equipped with full orders of their vertices. The edges will also be equipped with orientations, but that will rather be arbitrary. Specialized computer software, such as Mathematica[®] automatically supplies a predefined order and orientation for the simplices extracted from a triangulation. That fits perfectly well with our purposes.

The resonant mode carried by a p-simplex ξ will be specified in several ways:

$$|\xi\rangle = |[v_0, \dots, v_p]\rangle = (-1)^{\sigma}|[v_{\sigma(0)} \dots v_{\sigma(p)}]\rangle, \quad (1$$

where σ is any permutation and v_i are the vertices of the simplex. For example, for τ_1 from Fig. 2, we can take $v_0=\pi_1$, $v_1=\pi_2$ and $v_2=\pi_3$. On the other hand, if we choose $v_0=\pi_3$, $v_1=\pi_2$ and $v_2=\pi_1$, then $|[v_0,v_1,v_2]\rangle=-|\tau_1\rangle$. In other words, when the vertices appear in the pre-defined orientation, we refer to the actual mode, while otherwise we refer to the half-period delayed mode. At one point, we will need to present a simplex as a fully ordered sequence of vertices, in which case we write its mode as $|v_0,\ldots,v_p\rangle$. Lastly, the Hamiltonian will take the tight-binding form $\sum w_{\xi,\xi'}|\xi\rangle\langle\xi'|$, where the sum is over all simplices of the triangulation. We will use coupled-mode theory to implement this Hamiltonian with the collection of the resonators we just introduced.

One standard operation in combinatorial geometry is the boundary map, central to simplicial homology. This map lifts to our Hilbert spaces as

$$B|[v_0 \dots v_p]\rangle = \sum_{i=0}^p (-1)^i |[v_0 \dots \hat{v}_i \dots v_p]\rangle, \quad (2)$$

where hat indicates omission of that specific vertex. Note that, if the edges have the orientation induced by that of the face, as in the case of τ_1 in Fig. 2, then no negative signs occur in Eq. (2). However, this cannot be enforced throughout the triangulation and especially for neighboring facets. For example, negative signs do occur for τ_2 in

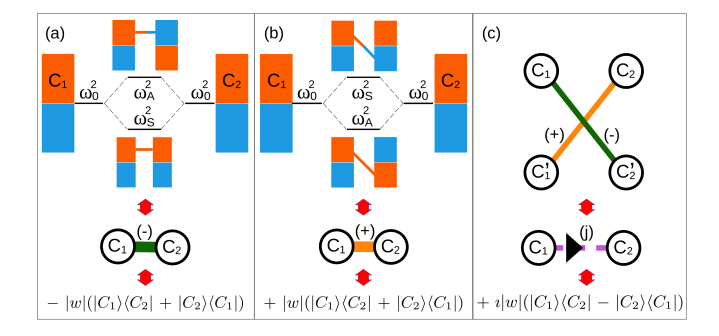


FIG. 4. Implementation of the hopping terms of a tight-binding Hamiltonian using bridged acoustic cavities (C) with fundamental frequency ω_0 . Each panel shows the physical connections (top), together with their symbols (middle) and the hopping terms (bottom) they implement. Panel (c) reduces a purely imaginary hopping term to the connections from panels (a) and (b), at the expense of introducing copies of the resonators (see main text). The value of $w = \frac{1}{2}(\omega_S^2 - \omega_A^2)$ can be adjusted by varying the cross section of the bridges. The coloring of the cavities is a rough representation of the air pressure field.

Fig. 2, for which $B|\tau_2\rangle = -|\epsilon_2\rangle + |\epsilon_4\rangle + |\epsilon_5\rangle$. For edges, the *B*-action takes $|[v_0, v_1]\rangle$ into $|[v_1]\rangle - |[v_0]\rangle$, and all vertices are sent to zero by *B*.

The matrix elements $\langle \xi | B | \xi' \rangle$ supply the strengths and signs of the couplings needed to implement the self-adjoint operator $B+B^{\dagger}$ with an actual meta-material. They are exemplified in Fig. 3 for the geometry and resonators from Fig. 2. As promised, these couplings engage only nearest-neighboring resonators and all have strengths equal to one [17]. There are, however, variations in the signs of the couplings, and we recall in Fig. 4 how such couplings are usually implemented with acoustic cavities.

Another operation in combinatorial geometry is the cap product of simplicial q-cocycles and (p+q)-cycles,

$$\psi \cap |[v_0, \dots, v_{a+p}]\rangle = \psi([v_p, \dots v_{a+p}]) |[v_0, \dots, v_p]\rangle, (3)$$

which can be adapted to our convention in (1) by antisymmetrization. It was observed in [10] that \smallfrown , together with the fundamental cycle $|X\rangle = \sum_{\tau} |\tau\rangle$ engaging all (ordered) 2-cycles of a triangulation, can be lifted to the Hilbert space as the linear operator

$$P|[\xi]\rangle := \bar{\delta}_{[\xi]} \smallfrown |X\rangle = \sum_{\tau} \bar{\delta}_{[\xi]} \smallfrown |\tau\rangle,$$
 (4)

where $\bar{\delta}_{[\xi]}$ is the signed delta function $\delta_{[\xi]}([\xi']) = \langle [\xi']|[\xi] \rangle$. This was used in [10] to construct the linear operator

$$T = \frac{1}{2}(P^{\dagger} + (-1)^{p}P), \tag{5}$$

which implements the Poincaré duality isomorphism, already mentioned in our introductory remarks, between the homologies of the dual Hilbert complexes

$$\mathcal{H}_0 \stackrel{B}{\leftarrow} \mathcal{H}_1 \stackrel{B}{\leftarrow} \mathcal{H}_2 \text{ and } \mathcal{H}_2 \stackrel{B^{\dagger}}{\leftarrow} \mathcal{H}_1 \stackrel{B^{\dagger}}{\leftarrow} \mathcal{H}_0.$$
 (6)

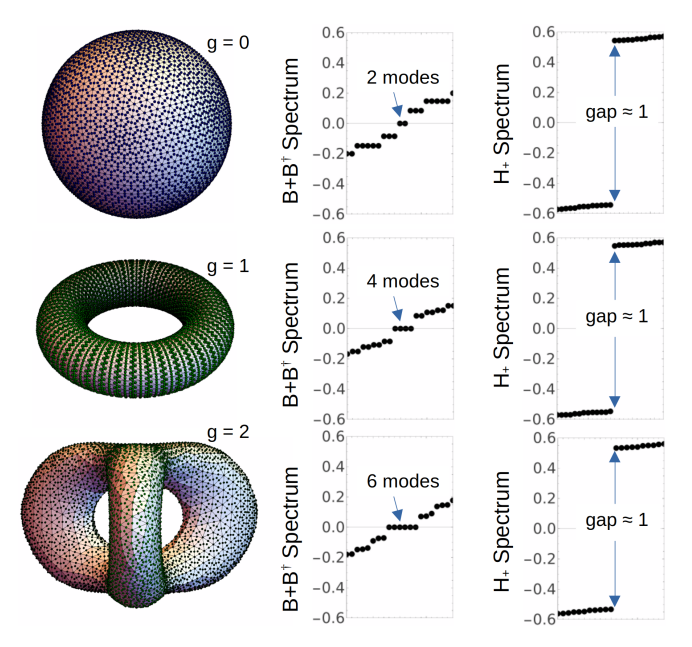


FIG. 5. The bulk spectra of the indicated operators when deployed on surfaces of different genus g. The number of zero modes of $B + B^{\dagger}$ confirms the relation (9). The features on these surfaces are placeholders for the resonators.

Lastly, T can be transformed into a self-adjoint operator $S=\imath^{p(p-1)+1}T$, which has the key property $BS+SB^\dagger=0$, assuring us that the Hamiltonians

$$H_{+} = B + B^{\dagger} \pm S \tag{7}$$

have spectral gaps at zero [9]. These are the two operators carrying Chern numbers ± 1 that were mentioned in our introduction.

The matrix elements $\langle \xi | S | \xi' \rangle$ are all pure imaginary and of magnitude $\frac{1}{2}$. They are exemplified in Fig. 3 for the geometry from Fig. 2. As advised in [18], we can promote $\sqrt{-1}$ to the matrix $j = \begin{pmatrix} 0 & 1 \\ -1 & 0 \end{pmatrix}$ and 1 to the 2×2 identity matrix, a move that removes the complex couplings at the expense of doubling the number of resonators (see Fig. 4(c)). The amplified Hilbert space $\mathbb{C}^2 \otimes \mathcal{H}$ comes equipped with a built-in symmetry, called U in [18], and, if we decompose the Hilbert space according to this symmetry, we have

Amplification of
$$H_{+} = \begin{pmatrix} H_{+} & 0 \\ 0 & H_{-} \end{pmatrix}$$
. (8)

Thus, as promised, we delivered an implementation of both topological models H_{\pm} with one metamaterial using only nearest-neighbor positive and negative couplings of strengths 1 or $\frac{1}{2}$ [19], in such a manner that their dynamics decouple and can be investigated independently (see [20] for further details).

Detecting the topology of the surface. The connected orientable surfaces are classified by their genus and, for a surface X of genus g, the singular homology groups

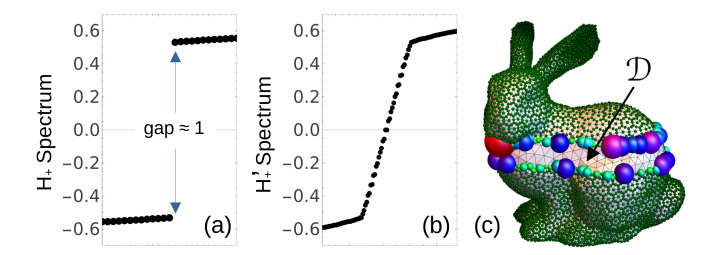


FIG. 6. (a) The bulk spectrum of the model when deployed on a triangulation of the Stanford Bunny. (b) The spectrum of the model when the resonators inside the domain \mathcal{D} are jammed. (c) The site amplitudes, encoded in the colors and radii of the balls, of a Gaussian packet $\sum_n e^{-\epsilon_n'^2/\sigma^2} \varphi_n'$, $\sigma = 0.6$, centered in the middle of the topological spectrum. Here, $\{\epsilon_n', \varphi_n'\}$ is the eigensystem of $H'_+ = H_+ + R_{\mathcal{D}}$.

are $H_0(X) \simeq H_2(X) \simeq \mathbb{Z}$ and $H_1(X) \simeq \mathbb{Z}^{2g}$. Being the boundary map for the singular complex, the zero modes of $B + B^{\dagger}$ coincide with the generators of the homology groups. As a consequence,

of zero modes =
$$2 + 2g$$
. (9)

Therefore, the operator $B+B^{\dagger}$ can be used to identify the topology of a surface when one is handed a file with a triangulation of that surface. This principle is exemplified in Fig. 5, which can be very useful in situations where the surface is very complex or it is folded many times and a global visualization is impossible. While this is not new as a mathematical subject [21], the interesting fact here is that we can actually "hear" the topology of the surface if we coat it with a metamaterial engaging the B-connections from Fig. 3.

Let us mentioned that the zero modes of $B+B^{\dagger}$ are spectrally separated from the rest of the modes only for finite triangulations. Indeed, as the triangulations are sequentially refined, the discrete spectra seen in Fig. 5 morph into gapless essential spectra. However, when we add the operator S, a clean spectral gap of approximate size one opens in the middle of the spectra and, in contrast to the previous situation, these gaps are stable against the refinements of the triangulations.

Topological edge modes. We are now ready to deliver our last promised feature, the generation of one-way topological wave-channels on the surface of real objects. For this, we implement H_+ on the triangulation from Fig. 1 and, to start, we confirm in Fig. 6(a) that the bulk spectrum is again gapped and free of defect-modes. The size of the gap is again approximately one.

Next, we add $R_{\mathcal{D}} = 10^6 \sum \chi_{\mathcal{D}}(\xi) |\xi\rangle\langle\xi|$, an onsite potential which effectively jams the dynamics inside the domain \mathcal{D} seen in Fig 6(c) (e.g. by flooding the resonators with water). In Fig. 6(b), we confirm that this action fills the entire bulk spectral gap with spectrum, which is a hallmark of Chern models. Furthermore, in Fig 6(c), a sampling of that spectrum reveals that the associated

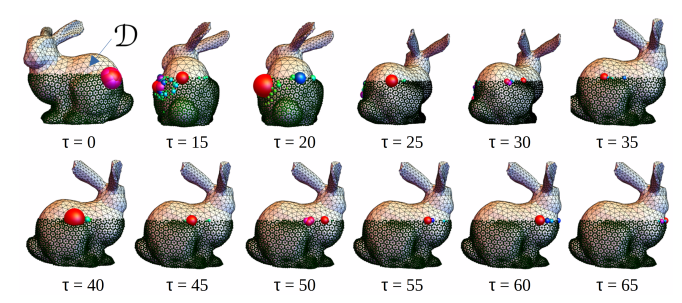


FIG. 7. Time evolution of the initial configuration seen in the frame t = 0, under the dynamics (10)generated by H'_{+} .

modes live at the boundary $\partial \mathcal{D}$ of the region \mathcal{D} .

In Fig 7 we chose the region \mathcal{D} to be the whole upper half-side of the object, and we consider an initial state $\psi(0)$ localized at the boundary $\partial \mathcal{D}$ (see first frame in Fig. 7). Its time evolution under the dynamics generated by $H'_{+} = H_{+} + R_{D}$ is sampled in the figure, confirming that the excitation sets in motion one and only one wavepacket which travels only in one direction along $\partial \mathcal{D}$. If we replace H_+ by H_- , we have verified that the there is again one and only one wave-packet which travels in the opposite direction. This confirms once again that the models H_{\pm} carry Chern numbers ± 1 . Another feature revealed by the simulations is the non-dispersive nature of topological modes, much desired in practical applications. Indeed, as the wave-packet travels in Fig. 7, it stays concentrated around its center of mass, as opposed to slowly flattening and spreading along the boundary.

The time evolution of the wave-packets was computed via exact diagonalization

$$|\psi(\tau)\rangle = \sum_{n} e^{i\epsilon'_n \tau} c_n |\varphi'_n\rangle, \quad H'_+ |\varphi'_n\rangle = \epsilon'_n |\varphi'_n\rangle, \quad (10)$$

and the c_n coefficients were extracted from the expansion $|\psi(0)\rangle = \sum_n c_n |\varphi_n\rangle$ of the initial state [22].

In conclusion, we devised an algorithm which takes the triangulation of a closed orientable surface at the input and coats the surface with a metamaterial whose dynamics displays a clean topological spectral gap carrying a non-trivial Chern number. The algorithm uses the matrix elements of the boundary and Poincaré duality operators, which are available in universal forms for any Hilbert complex derived from triangulations of closed oriented surfaces. We confirmed that, after removing or jamming the resonators in a region of the surface, one-way propagation channels develop along the boundary of the region. Our findings represent an important step towards deploying topological metamaterials on the surfaces of real-world objects, hence bringing the topological metamaterials closer to real-world applications.

Acknowledgments. This work was supported by the U.S. National Science Foundation through grants CMMI-2131760 and DMS-1952669, and from the U.S. Army Research Office through contract W911NF-23-1-0127.

- * higson@psu.edu † prodan@yu.edu
- F. D. M. Haldane, Model for a Quantum Hall-Effect without Landau levels: Condensed-matter realization of the parity anomaly, Phys. Rev. Lett. 61, 2015-2018 (1988).
- [2] A. P. Schnyder, S. Ryu, A. Furusaki, A. W. W. Ludwig, Classification of topological insulators and superconductors in three spatial dimensions, Phys. Rev. B 78, 195125 (2008).
- [3] X.-L. Qi, T. L. Hughes, Shou-Cheng Zhang, Topological field theory of time-reversal invariant insulators, Phys. Rev. B 78, 195424 (2008).
- [4] A. Kitaev, Periodic table for topological insulators and superconductors, (Advances in Theoretical Physics: Landau Memorial Conference) AIP Conference Proceedings 1134, 22-30 (2009).
- [5] S. Ryu, A. P. Schnyder, A. Furusaki, A. W. W. Ludwig, Topological insulators and superconductors: tenfold way and dimensional hierarchy, New J. Phys. 12, 065010 (2010).
- [6] E. Prodan and H. Schulz-Baldes, Bulk and boundary invariants for complex topological insulators: From K-theory to physics, (Mathematical Physics Studies, Springer, 2016).
- [7] A refinement will be followed by a scaling of the surface such that the scale of the triangles remain unchanged.
- [8] https://graphics.stanford.edu/data/3Dscanrep/
- [9] N. Higson, J. Roe, Mapping surgery to analysis I: Analytic signatures, K-Theory 33, 277–299 (2004).
- [10] N. Higson, J. Roe, Mapping surgery to analysis I: Geometric signatures, K-Theory 33, 301–324 (2004).

- [11] N. Higson, J. Roe, Mapping surgery to analysis III: Exact sequences, K-Theory 33, 325–346 (2004).
- [12] Supplemental Materials.
- [13] C. T. C. Wall, Surgery on compact manifolds, (AMS, Providence, 1999).
- [14] N. P. Mitchell, L. M. Nash, D. Hexner, A. Turner, W. T. M. Irvine, Amorphous topological insulators constructed from random point sets, Nat. Phys. 14 380–385 (2018).
- [15] C. Bourne, E. Prodan, Non-commutative Chern numbers for generic aperiodic discrete systems, J. Phys. A: Math. Theor. 51, 235202 (2018).
- [16] C. Bourne and B. Mesland, Index theory and topological phases of aperiodic lattices, Ann. Henri Poincaré 20, 1969-2038 (2019).
- [17] Note that the energy scale is set by the resonant frequency of the uncoupled resonators.
- [18] Y. Barlas, E. Prodan, Topological classification table implemented with classical passive metamaterials, Phys. Rev. B 98, 094310 (2018).
- [19] If desired, the coupling strengths can be forced to be one, by replacing H_+ with $B + B^{\dagger} + 2S$.
- [20] S.-Q. Wu, W. Cheng, X.-Y. Liu, B.-Q. Wu, E. Prodan, C. Prodan, J.-H. Jiang, Observation of D-class topology in an acoustic metamaterial, Science Bulletin 69, 893–900 (2004).
- [21] T. Kaczynski, K. Mischaikow, M, Mrozek, Computational Homology, (Springer, New York, 2004).
- [22] For the classical metamaterial, the eigenmodes evolve in time as $\varphi'_n(t) = e^{\imath \omega'_n t} \varphi'_n$ rather than $\varphi'_n(t) = e^{\imath \epsilon'_n t} \varphi'_n$, but the expansion $\omega'_n = \omega_0 \sqrt{1 + \epsilon'_n/\omega_0^2} \approx \omega_0 + \frac{1}{2} \epsilon'_n/\omega_0$, $\epsilon'_n = \omega'_n^2 \omega_0^2$, justifies (10) if τ there stands for $t/2\omega_0$. The factor $e^{\imath \omega_0 t}$ does not affect the plotted amplitudes. This is standard in the coupled-mode theory, which is valid in the regime $\epsilon/\omega_0^2 \ll 1$.